C: Surfaces, Interfaces, Porous Materials, and Catalysis

Can Single Metal Atoms Trapped in Defective h-BN/Cu (111) Improve Electrocatalysis of the H Evolution Reaction?

Daniele Perilli, Cristiana Di Valentin, and Felix Studt

J. Phys. Chem. C, **Just Accepted Manuscript** • DOI: 10.1021/acs.jpcc.0c06750 • Publication Date (Web): 29 Sep 2020

Can Single Metal Atoms Trapped in Defective h-BN/Cu (111) Improve Electrocatalysis of the H_2 Evolution Reaction?

Daniele Perilli,[1] Cristiana Di Valentin[1] and Felix Studt[2,3]

[1] Department of Materials Science, University of Milano-Bicocca, via Cozzi 55, 20125 Milano, Italy

[2] Institute of Catalysis Research and Technology, Karlsruhe Institute of Technology (KIT), Hermann-von-Helmholtz-Platz 1, D-76344 Eggenstein-Leopoldshafen, Germany

[3] Institute for Chemical Technology and Polymer Chemistry, Karlsruhe Institute of Technology (KIT), Engesserstraße 18-20, D-76131 Karlsruhe, Germany

Abstract

Metal-supported hexagonal boron nitride monolayers (h-BN/M) are emerging as new potential electrocatalysts for various energy-related oxidation or reduction processes. So far, several preparation methods have been developed to introduce, in a controlled way, defects such as vacancies or substitutional heteroatoms. Herein, we investigate by dispersion-corrected density functional theory (DFT) calculations defective and metal-doped h-BN/Cu(111) systems as electrocatalysts for the hydrogen evolution reaction (HER). By calculating the hydrogen binding energy (ΔG_{*H}) at different coverage conditions, we observe how the interaction between the defective/metal-doped h-BN layer and the Cu(111) substrate plays a key role in tuning the reactivity, leading to a thermoneutral hydrogen adsorption step (i.e. $\Delta G_{*H} \approx 0$). These results could be generalized to other h-BN/M interfaces and may help their rational design for an improved H_2-evolving electrocatalysis.

1. INTRODUCTION

The use of molecular hydrogen (H_2) as an energy carrier is considered a viable alternative to fossil fuels for the energy supply.[1,2] However, H_2 does not exist naturally on Earth and must be produced in a cost-effective way. Nowadays most of the hydrogen is obtained industrially by steam reforming, which employs fossil fuels, emits carbon dioxide, and produces H_2 of low purity. An alternative clean and renewable route towards the production of pure molecular hydrogen is the direct water splitting,[3] which is an uphill reaction but can be conducted electrochemically, thus potentially stemming from renewable sources, such as wind and solar.[4,5]

Hydrogen evolution is a two-electron reduction process that can follow two possible mechanisms: a) the *Volmer−Heyrovsky* and b) the *Volmer−Tafel* paths, which consist of the following sets of reaction steps (in acidic media):

a) *Volmer−Heyrovsky* path

$$* + (H^+ + e^-) \rightarrow *H \qquad (a1)$$

$$*H + (H^+ + e^-) \rightarrow * + H_{2,(g)} \qquad (a2)$$

b) *Volmer−Tafel* path

$$* + (H^+ + e^-) \rightarrow *H \qquad (b1)$$

$$*H + *H \rightarrow * + H_{2,(g)} \qquad (b2)$$

where * is a catalytic site and *H is a surface−bound hydrogen.

Since both mechanisms share the first electrochemical step (*Volmer*), previous theoretical works have identified the free binding energy of a hydrogen atom (ΔG_{*H}) as a simple descriptor of the electrocatalytic performance.[6,7] In fact, according to the *Sabatier* principle, the interaction between the catalyst and the adsorbate should be "just right"; that is, neither too strong nor too weak. If the interaction is too weak, a high overpotential will be required to bind H and no reaction will take place at a reasonable potential. On the other hand, if the interaction is too strong, the adsorbed H atoms will poison the catalyst and no H_2 will be formed. Thus, the optimum condition

is satisfied when the binding of H atoms is close to thermoneutrality, i.e. $\Delta G_{*H} \approx 0$. Taking this simple approximation, it is possible to correlate the electrocatalytic activity with the thermodynamic parameter ΔG_{*H}, which can be calculated rather easily with quantum chemical methods such as DFT. This analysis allowed a rationalization of the reactivity trends among different catalysts (as e.g. expressed through so-called volcano relationships),[7] but also to identify and predict potential new systems. However, it is worth to highlight how thermoneutrality is a necessary but not sufficient condition for a catalyst to be active for HER.[8]

Currently, state-of-the-art electrocatalysts in acidic media are mainly based on platinum and its alloys, which are rare, and costly, and therefore not suitable for large-scale use. For all these reasons, intense scientific efforts are devoted to search for an efficient, inexpensive, stable H_2-evolving electrocatalyst for the HER.[9] An emerging class of electrocatalysts, that have the potential to meet the above mentioned requirements, are two-dimensional (2D) materials.[10,11,12,13,14] For example, (10-10) Mo-edges in MoS_2 nanocrystals were found to be active sites for the electrochemical hydrogen evolution, both experimentally[15,16] and theoretically.[17,18,19] Also, in combined experimental and theoretical work, a metal-free hybrid system, made by coupling of graphitic-carbon nitride with nitrogen-doped graphene (g-C_3N_4@NG), was found to be an active electrocatalyst for the hydrogen evolution reaction.[20]

Another important 2D material that could be of potential interest for electrocatalysis is metal-supported hexagonal boron nitride (h-BN). Although pristine h-BN is intrinsically insulating and inert, when it is chemically modified by dopants, defects, or underlying metal substrates, its reactivity and band gap can be tuned.[21,22,23,24,25,26,27,28] For example, combining experiments and DFT calculations, Au-supported h-BN nanosheets were successfully studied for the oxygen reduction reaction (ORR)[29] and HER,[30] and h-BN edges were proposed to be the active sites for both processes. Recently, Liu et al. experimentally compared the performance of h-BN nanosheets on Cu (h-BN/Cu) and Au (h-BN/Au) and found that the interaction with the underlying metal substrate plays a key role in tuning the electrochemical activity.[31]

An alternative strategy to activate h-BN, and more generally 2D materials, is by metal doping. These isolated metal atoms could be potentially active sites for several catalytic and electrocatalytic processes, as previously observed in several theoretical works.[32,33,34,35] Different methods were developed to dope *ad hoc* 2D materials, such as ion implantation or e-beam

evaporation from metal rods.[36] However, also impurities and adatoms already present on the metal surface could be incorporated into the 2D layer during its growth by chemical vapor deposition (CVD), as previously proved for epitaxial graphene on the Ni(111) surface.[37,38]

In our previous works, we analyzed the electronic interaction between a pristine and defective h-BN monolayer on a Cu(111) substrate[39] and we studied these interfaces as potential electrocatalysts for the oxygen evolution reaction.[40]

In the present work, we investigate whether defective (N and B monoatomic vacancies, and BN diatomic vacancy) and metal-doped (Cu, Ni, Co, and Fe) Cu-supported h-BN systems may be of potential interest for HER. We first analyze the structural and electronic properties and stability of such interfaces. Then, by computing the H binding energy at different coverage conditions, we evaluate the performance of these h-BN/Cu hybrid systems as electrocatalysts for the hydrogen evolution reaction.

2. COMPUTATIONAL DETAILS

Density Functional Theory (DFT) calculations were performed using the plane-wave-based Quantum ESPRESSO package (QE).[41,42] The ultrasoft pseudopotentials[43] were adopted to describe the electron-ion interactions with Cu (3d, 4s), Ni (3d, 4s), Co (3d, 4s), Fe (3d, 4s), B (2s, 2p), N (2s, 2p) and H (1s) treated as valence electrons. Energy cutoffs of 30 Ry and 240 Ry (for kinetic energy and charge density expansion, respectively) were used for all calculations. The convergence criterion of 0.026 eV/Å for forces was used during geometry optimization and the convergence criterion for the total energy was set to 10^{-6} Ry. To properly take into account weak interactions, the van der Waals density functional vdW-DF2^{C09x} was used.[44,45] Spin polarization was considered when required.

For the simulation of h-BN/Cu(111) interfaces, a (6 × 6) supercell with a total of 108 Cu atoms and 72 atoms in the BN layer was used resulting in a lattice mismatch of only 0.40 %. The Cu(111) surface was modeled by a three-layer slab model with the bottom two layers fixed during the geometry relaxation to mimic a semi-infinite solid. A Monkhorst-Pack[46] k-points mesh of 3 × 3 × 1 and 9 × 9 × 1 was used for the geometry relaxation and density of states (DOS) evaluation, respectively. To avoid interactions between adjacent periodic images, a vacuum space of about 25 Å was included in the slab model.

The free energies (G) of the intermediates (at T = 298.15 K) were computed by correcting the electronic energies (E) for the zero-point energy (ZPE), heat capacity ($\int C_p dT$) and the vibrational entropic term (S_{vib}), calculated as follows:

$$G = E + ZPE + \int C_p dT - TS_{vib}$$

Vibrational modes were calculated by performing a normal-mode analysis and all 3N degree of freedom of the adsorbates within the harmonic oscillator approximation. Corrections for the ZPE were included by calculating and diagonalizing the dynamical matrix in *Gamma* point only. For a gas-phase H_2 molecule, the standard tabulated entropy was used.[47]

The electrochemical cell was simulated using the Computational Hydrogen Electrode (CHE) model originally proposed by Nørskov and co-workers.[48] The Climbing Image−Nudged Elastic Band (CI−NEB)[49] method was employed to simulate the *Tafel* step at the Cu−supported defective h-BN, generating the minimum energy path of the reaction step and an evaluation of the energy barrier. A Löwdin population analysis,[50] as implemented in the QE package, was used to calculate the partial atomic charges. Ball-and-stick models were rendered with Xcrysden software.[51]

3. RESULTS AND DISCUSSION

3.1. Structural and electronic properties of metal-doped defective h-BN/Cu(111) systems.

We previously observed that B vacancies, presenting N-terminated triangular holes in the lattice, can encapsulate Cu adatoms owing to the large stabilization effect deriving from the Cu-N bond formation.[39] Therefore, we first considered the monoatomic B vacancy as the "trapping site" for a range of light transition metal atoms (M): Cu, Ni, Co, and Fe. According to the most stable stacking configuration for the h-BN layer on top of the Cu surface, where N/B atoms are in top/fcc position with respect to the Cu substrate, we considered only the fcc position for the extra metal atom.

We will consider two slightly different situations for the trapped M atoms: (1) the M atom is in the interfacial region where it is still in contact with the underlying surface but is also bound to the undercoordinated N atoms in the defective h-BN layer (M^{down}@1Vac, Figure 1a); (2) the M atom is exposed towards the vacuum and does not have any contact with the underlying copper substrate (M^{up}@1Vac, Figure 1b).

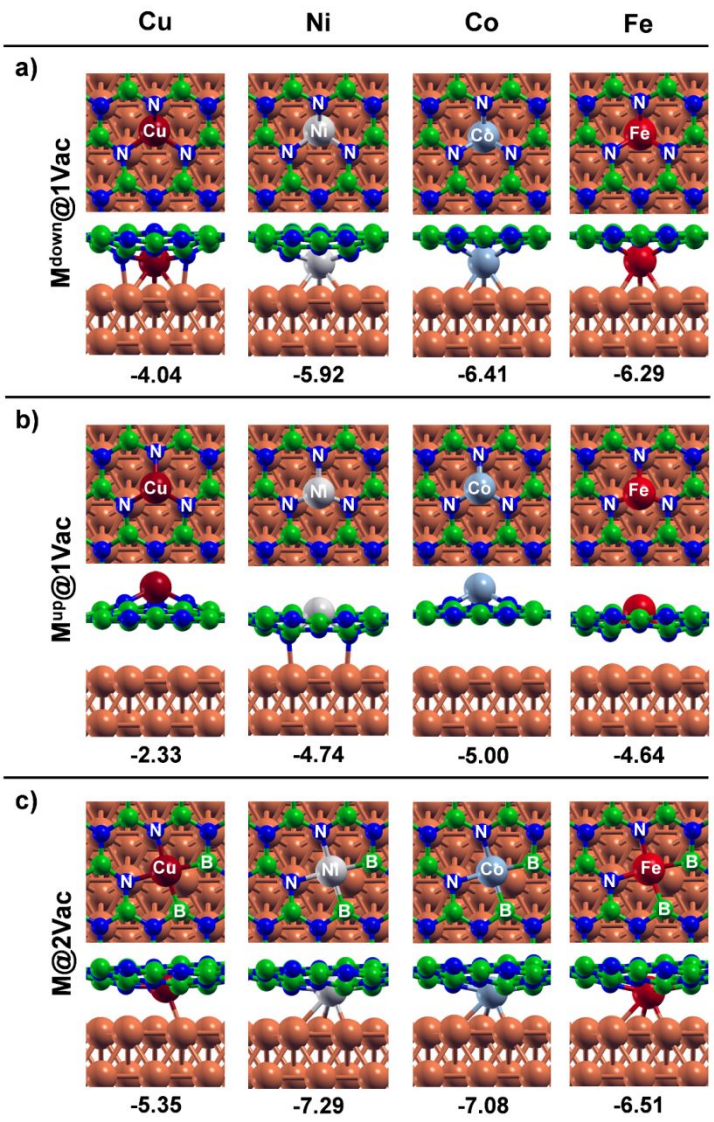

Figure 1. Top and side views for supported metal-doped h-BN in a single B vacancy (1Vac) with the embedded metal in (a) down and (b) up configuration, and into a (c) BN divacancy (2Vac). The corresponding formation energies are reported below each configuration. The formation energies are given relative to the corresponding metal atom in the gas−phase. Color coding: Cu surface atoms in orange, N atoms in blue, B atoms in green, and Cu, Ni, Co, and Fe trapped atoms in dark red, gray, cyan and red, respectively.

The M atoms tend to go either up or down because they are quite large and do not perfectly fit in the spatial hole left by the missing B atom. We could not localize a minimum energy structure with the M atom at the same height of the h-BN plane. Therefore, we decided to consider a larger vacancy (diatomic vacancy) where a BN atomic pair is missing, as shown in Figure 1c (M@2Vac).

Even for this double vacancy model, all optimized structures show a significant distortion of the 2D layer, and the M atom is always closer to the Cu surface than the h-BN layer.

Next, we evaluated whether there is an energy cost or gain to go from a defective supported h-BN/Cu layer and trap a single M atom to form the M@1Vac/2Vac structure, according to the following equation:

$$E_F = E_{M@1Vac/2Vac} - E_{1Vac/2Vac} - E_{M-atom} \qquad (1),$$

where $E_{M@1Vac/2Vac}$, $E_{1Vac/2Vac}$, and E_{M-atom} are the total energies of the M-filled vacancy, empty vacancy, and the isolated metal atom, respectively. This energy change is always negative, although in the case of M^{up}@1Vac, the energy gain is considerably smaller. We rationalize this trend as a consequence of the fact that when the metal is in the up configuration, its interaction with the Cu substrate is completely suppressed. On the contrary, in the down configuration, the stabilization comes from the formation of bonds both with the undercoordinated N atoms from the defective h-BN layer and with the underlying Cu surface atoms.

In order to get further insight into the nature of the different trapped M atoms, we have analyzed and compared their electronic structure in terms of the total and projected density of states (DOS and PDOS; Figure S1 and S2) of the d states of the embedded M atoms. In the case of the Cu^{down}@1Vac and Ni^{down}@1Vac systems, the d states associated with the single metal atom show a significant broadening due to the strong coupling with the Cu substrate and have a considerable fraction near the Fermi energy. On the contrary, in the case of the Co^{down}@1Vac and Fe^{down}@1Vac systems, the metal d states show a narrow peak in the proximity of the Fermi energy resembling a similar electronic structure as isolated or single metal atom catalyst.[52] Interestingly, only Ni- and Fe-doped systems, in the down atomic configuration, show a residual magnetization after optimization, with a total magnetic moment per cell of 0.69 μ_B and -1.71 μ_B, respectively. By analyzing the atomic spin density values, such magnetic moment is found to be mainly localized on the trapped metal atoms.

For the systems with a double vacancy, M@2Vac (Figure S2), we note that all projections exhibit less broadening compared to the mono vacancy cases, indicating smaller interactions with the Cu substrate: the Cu d-states are at a low energy (at least below -2 eV), the Ni and Co d-states show a full sharp peak close to the Fermi level (especially in the case of Co), whereas, in the case of Fe, we observe an empty narrow peak in the alpha channel (spin up electrons). Only in the latter

case, we found a magnetic ground state, with a total magnetic moment per cell of -0.65 μ_B, which is mainly localized on the Fe atom.

We performed a Löwdin population analysis and found that the embedded metal atoms are positively charged due to an electron transfer to the Cu slab. Interestingly, we found that the amount of transferred charge is significantly lower for M@2Vac than for M@1Vac (as shown in Figure 2a).

As pointed out above, the electrochemical stability is another important condition to be satisfied by potential new electrocatalysts. For this reason, we investigated the stability of the trapped M atoms against the dissolution in water, according to a previously employed methodology,[26,33,53] as detailed in the S.I. Figure 2b and c shows the calculated dissolution potential of trapped metals ($U_{diss(M@V)}$) as a function of the formation energies, as calculated with respect to an isolated (Figure 2b) and bulk-phase (Figure 2c) metal atom. Since the working potential to evolve $H_{2,(g)}$ is always negative (with respect to SHE), a positive dissolution potential will guarantee the stability of the trapped metal to its dissolution in water under electrochemical conditions. Therefore, systems in the upper left quadrant of Figure 2 ($U_{diss(M@V)} > 0$ V and formation energy < 0 eV) are promising in terms of stability.

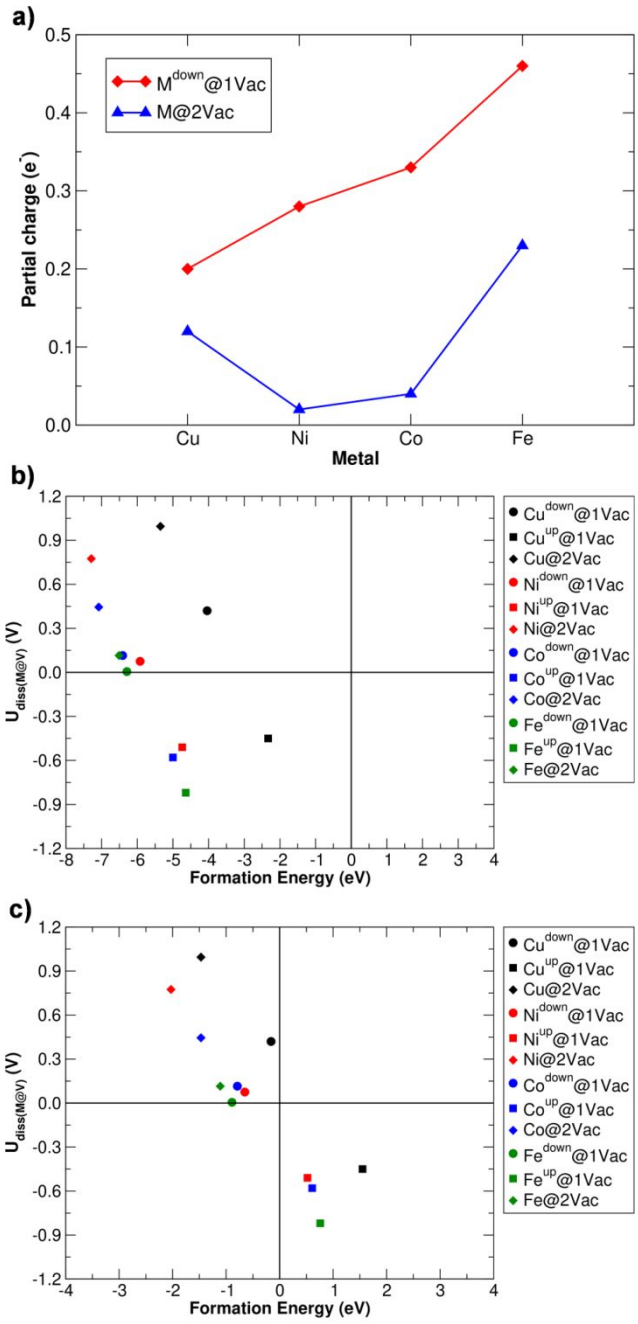

Figure 2. (a) Partial charges of trapped metals for M^{down}@1Vac and M@2Vac systems. Dissolution potentials (with respect to SHE and pH = 0) of trapped metals ($U_{diss(M@Vac)}$) plotted versus formation energies as calculated with respect to an (b) isolated and (c) bulk-phase metal atom.

It is interesting to note that all M^{up}@1Vac structures lie in the third quadrant and are therefore not stable, based on the criterion of electrochemical stability. Again, this is due to the absence of the

interaction of the trapped metal atom with the underlying Cu substrate, which reduces the overall stability of the system.

In addition to the energy and electrochemical stability, we also considered the activation barrier for Cu and Ni atoms to pass through the B monovacancy, moving between the up (M^{up}@1Vac) and down (M^{down}@1Vac) structures. As shown in Figure S3, it is interesting to note that all M^{up} structures are not only significantly less stable than their M^{down} counterparts, but the energy barriers from M^{up} to M^{down} are also very small (~0.1 eV). M^{up} structures are thus not catalytically relevant and will hence not be considered any further.

To conclude this section, we present the analysis, limited to the case of M^{down}@1Vac, of the interaction between M and the three coordinating N atoms. For this, the use of formation energy values, as defined above, is not suitable to compare the strength of the N-M bonds for the following reasons: (1) the formation energy takes the different deformation contributions into account due to both the atomic structural distortions and the change in adhesion strength between h-BN and Cu; (2) in the formation energy both the contributions of the metal atom interaction with the Cu substrate and with the BN-layer are present and cannot be easily separated. The first problem can be solved by employing a simple scheme of energy decomposition, as we used in our previous work.[39] As shown in Figure 3a, this decomposition allows one to determine the energy contribution of deformation (positive, ΔE_{def}) and of binding (negative, ΔE_{bind}) to the adsorption energy ($\Delta E_{ads} = E_{M@1Vac} - E_{1Vac} - E_{M-atom}$) of M^{down}@1Vac (for the values see Table S2). Now, comparing the binding energies (ΔE_{bind}) obtained for the different metal-doped systems, we determined the following order of trapped metal atom stability , from the least to the most stable: Cu (-5.66 eV), Ni (-7.70 eV), Fe (-9.02 eV), and Co (-9.06 eV).

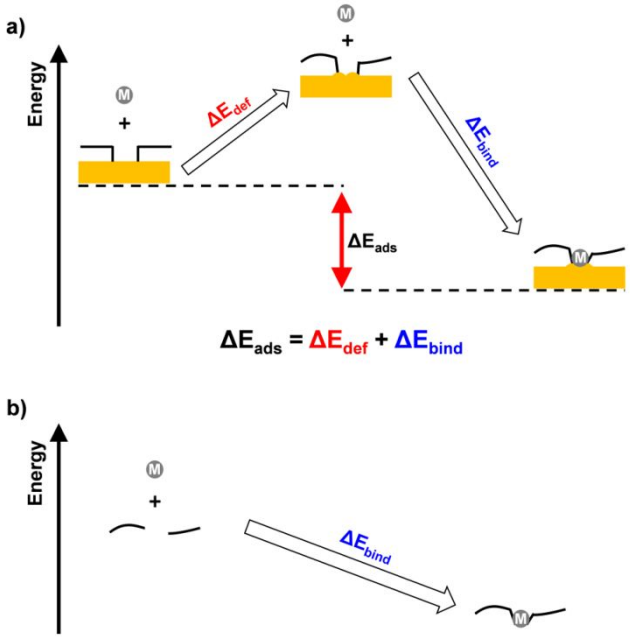

Figure 3. (a) Schematic representation of the energy decomposition analysis for the energy contribution of deformation (positive, ΔE_{def}) and of binding (negative, ΔE_{bind}) to the adsorption energy (negative, ΔE_{ads}) of the metal trapping in h-$B^{V}N$/Cu(111) interface.[39] (b) Schematic representation of binding energy contribution deriving from the formation of N-M bonds.

As regards the second problem, to roughly estimate only the bonding contribution to the N atoms, we calculated the binding energy of a metal atom trapped in a free-standing h-$B^{V}N$ layer, which is distorted as when lying over the Cu substrate, according to the scheme reported in Figure 3b. The M-N bond was estimated to increase as follows: -2.24 eV per Cu-N, -2.88 eV per Ni-N, -2.95 eV per Fe-N, and -3.14 eV per Co-N.

3.2. Assessment of the HER on defective and metal-doped h-BN/Cu(111) interfaces.

Defect−free h-BN/Cu(111) was suggested to be a good ORR catalyst based on theoretical calculations.[21] While we do not necessarily expect that the same is true for HER, we will use h-BN/Cu(111) as our reference system.

We evaluate the stability of the H* intermediates of the HER in terms of Gibbs free energy as:

$$\Delta G_{*nH} = G_{*nH} - G_{*} - \frac{n}{2} G_{H_{2,(g)}} \qquad (2)$$

where G_{*nH}, G_{*}, and $G_{H_{2,(g)}}$ are the Gibbs free energies for the catalyst with n hydrogen atoms adsorbed, the catalyst without any hydrogen atom, and an isolated H_2 molecule in the gas−phase, respectively. From now on, we will refer to this quantity as the *hydrogen binding energy*.

Another way to evaluate the stability of the *H intermediates is through the *differential hydrogen binding energy*, which is the energy cost or gain to gradually increase the H* coverage, and is calculated as follows:

$$\Delta G_{*H}^{diff} = G_{*nH} - G_{*(n-1)H} - \frac{1}{2} G_{H_{2,(g)}} \qquad (3)$$

In the case of defect−free h-BN/Cu (Figure S4), we found the electrochemical H adsorption to be unfavorable (ΔG_{*1H} = +1.27 eV), with the H bonded to a B atom (see Figure S5). This result agrees well with what has been reported from experiments[31] and suggests that the rather weak interaction between the Cu substrate and the h-BN layer does not alter the activity of h-BN to a great extent (ΔG_{*1H} =+2.41 eV in the case of free-standing h-BN, Figure S5).

In the following subsections, we present the investigation of the HER mechanism for different defective and metal−doped h-BN/Cu systems using the computational hydrogen electrode (CHE) model.[48] For HER the most optimal electrocatalyst should have a *differential hydrogen binding energy* close to zero, i.e. $\Delta G_{*H}^{diff} \approx 0$ eV. As mentioned above, if the interaction is too weak ($\Delta G_{*H}^{diff} \gg 0$), a high overpotential will be required for the first proton/electron transfer process, whereas, if the interaction is too strong ($\Delta G_{*H}^{diff} \ll 0$), the adsorbed H bind too strongly, making the second proton/electron transfer step difficult. Thus, the thermoneutrality of this step is a necessary but not sufficient condition for a catalyst to be active for the HER.

3.2.1. Empty mono- and di-atomic vacancies

Point defects, such as vacancies, in h-BN are considered to improve its reactivity. When one atom is removed from the h-BN lattice, the monolayer contains some undercoordinated atoms, which become very reactive. Here we will investigate if this translates into a positive effect on the catalyst activity for HER.

We start considering the case of a boron monovacancy in free-standing h-BN (h-B^VN, Figure 4 and 5a), where the three nitrogen atoms at the vacancy site are truly undercoordinated (in contrast with the case on a Cu substrate where they can form bonds with the surface Cu atoms in Figure 5b) and prompt to form new bonds. Because of that, the binding energy for the first H atom added to the free-standing system is higher than in the corresponding Cu-supported h-B^VN. The increase in H coverage by further addition of H atoms leads to comparable energy gains for the various reaction steps (≈ 2 eV). In other words, without an underlying substrate, it is not possible to reach the thermoneutrality since there is nothing able to damp the huge energy gain due to the formation of N-H bonds. Nevertheless, the type of substrate also plays a crucial role to tune the H adsorption, as we can see by comparing the case of h-B^VN supported on Cu(111) with that on Ni(111), which do not agree (Figure S6).

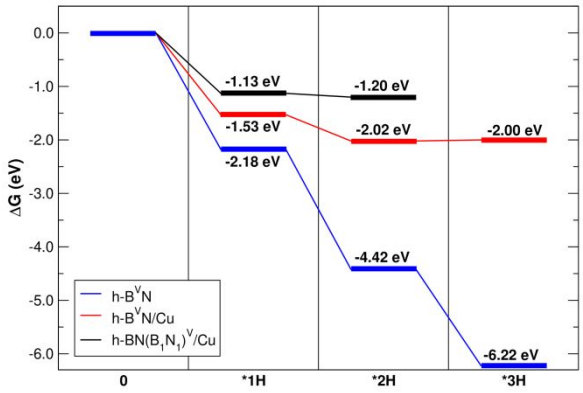

Figure 4. Free-energy diagram (ΔG) for the electrochemical hydrogen adsorption catalyzed by defective Cu-supported h-BN systems and coverage-dependence.

Next, we analyze and compare the boron (h-B^{V}N/Cu) and the nitrogen (h-BN^{V}/Cu) monovacancy (red and green lines in Figure 4 and S4, respectively), with the BN divacancy (h-BN(B$_1$N$_1$)^{V}/Cu, black line in Figure 4). The B (N) vacancy induces three undercoordinated N (B) atoms, whereas the BN divacancy gives rise to four undercoordinated N/B atoms (Figure 5b, S5 and 5c, respectively). However, in all cases, the undercoordinated B/N atoms are passivated by Cu surface atoms, forming strong B/N-Cu covalent bonds, as we have detailed in a previous work.[39]

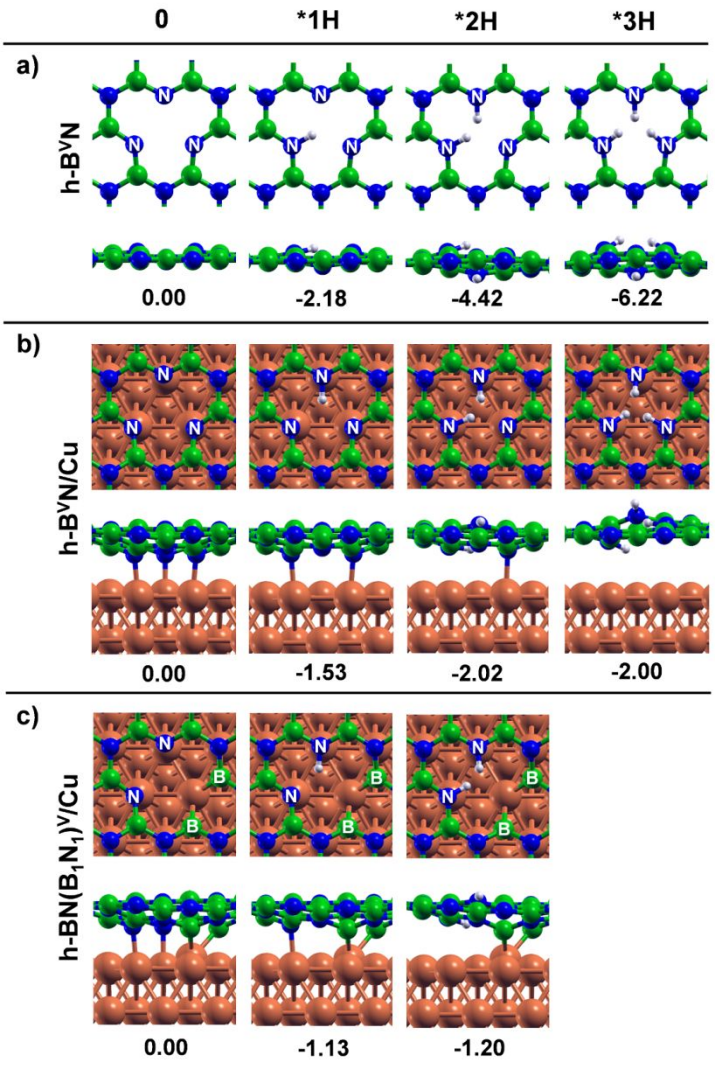

Figure 5. Top and side views of the intermediates of the hydrogen adsorption on (a) free standing and (b) Cu-supported B monovacancy, and (c) Cu-supported BN divacancy, as shown in Figure 4.

The corresponding hydrogen adsorption energies (ΔG_{*nH}), are reported below each structure. Color coding: Cu surface atoms in orange, N atoms in blue, B atoms in green, and H in white.

In the case of h-BN^{V}/Cu, we calculate ΔG_{*1H} = +1.32 eV (Figure S4), with the H atom that does not bind to an undercoordinated B atom of the vacancy site but to an N atom next to the vacancy, resembling the pristine h-BN/Cu case (see Figure S5).

For h-B^{V}N/Cu, we calculate a binding energy of -1.53 eV ($\Delta G_{*1H} = \Delta G_{*H}^{diff}$) for the first coupled proton/electron transfer step. The optimized geometry (second panel in Figure 5b) shows the formation of an N-H bond accompanied by a breaking of the previous interfacial N-Cu bond. The energy cost to break one bond is thus compensated by the large energy gain for the formation of the other. While the adsorption of the first hydrogen is rather strong, the calculated differential hydrogen adsorption energy (ΔG_{*H}^{diff}) decreases with an increase of adsorbed hydrogen and is only -0.49 eV and +0.02 eV for the second and third proton/electron transfer step. We rationalize this by the cost of breaking the Cu-N bonds and by the steric repulsion between H atoms, which is increasing with the increase in the number of H atoms. This is confirmed by the observation in Figure 5b that the N-H bonds are pointing out from the BN layer, either up or down, causing some distortion. It is interesting to note in Figure 4 that the differential hydrogen adsorption energy for the third step is calculated to be thermoneutral (+0.02 eV). The calculations thus indicate that h-B^{V}N/Cu is a formidable HER catalyst, with the resting state (i.e. the state before thermoneutral reaction step) having 2 H* adsorbed.

For the double vacancy, h-BN(B$_1$N$_1$)^{V}/Cu (black line in Figure 4), our results are similar to the single B vacancy (red line): H binds to an undercoordinated N atom of the vacancy in a too stable intermediate (ΔG_{*1H} = -1.13 eV) for a catalytic process. Since we only have two "undercoordinated" N atoms, there are only two proton/electron transfer steps possible. The second is just slightly lower in energy by –0.07 eV, as shown in Figure 4 (black line). On this basis, the activity by this defect site (BN divacancy) is predicted to lead to a good HER performance.

In order to get some insight into the kinetic aspect of the processes discussed in this section, we have also estimated activation barriers (by performing CI-NEB calculations) to suggest a possible

reaction mechanism for the hydrogen evolution. Since *Heyrovsky* barriers are rather challenging to be computed for our systems, only *Tafel* barriers were investigated in the present work (Figure S7). In the case of h-$B^{V}N$/Cu, the activation barrier for the Tafel reaction was estimated to be as high as 2.71 eV (Figure S7b). On this basis, we would reasonably exclude a *Tafel* mechanism for the hydrogen evolution reaction, and hypothesize a *Heyrovsky* mechanism, in analogy to what previously observed for MoS_2-based catalysts, where activation barriers are found to be ≈ 0.8 eV.[18,19]

3.2.2. Trapped single metal atoms in mono- and di-atomic vacancies

Isolated metal atoms, trapped in a defective h-BN lattice, could be potential active sites for electrocatalysis, as observed in our previous work.[40]

For the case of the metal atom trapped in a B monovacancy (M@1Vac in Figure 6a), we made several unsuccessful attempts to locate a structure with the H binding directly to the metal. This might be due to the low position of the metal atom with respect to the plane of the h-BN layer, which makes it rather inaccessible for reaction from the top side. The H atoms bind to the undercoordinated N atoms at the vacancy site, gradually decoupling the metal adatom from the BN layer. Due to this, at high H coverage, the metal atom moves to a next hcp site to allow full relax of the N-H bonds.

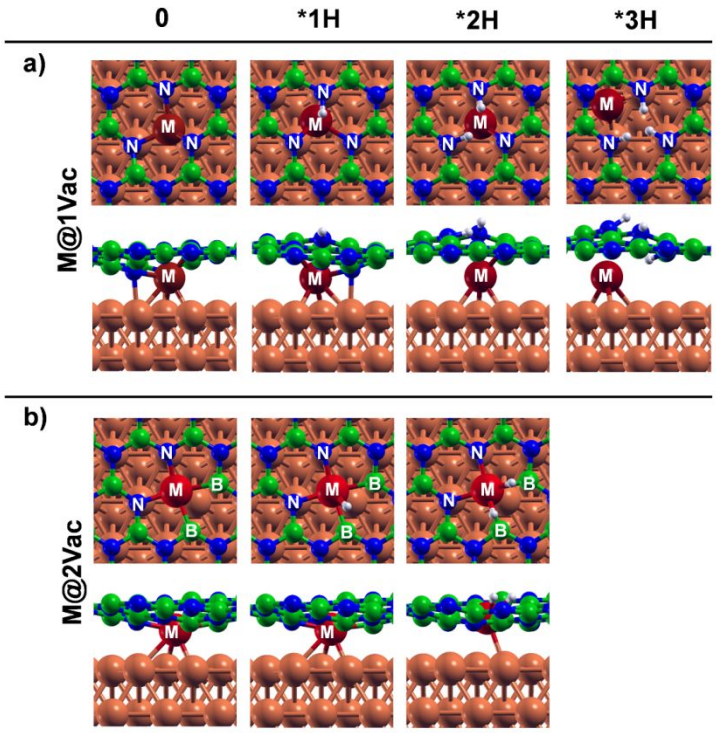

Figure 6. Top and side views of the intermediates of the hydrogen adsorption on supported M-doped h-BN systems: (a) M in a B monovacancy and (b) M in a BN divacancy, as shown in Figure 7a and b, respectively. Color coding: Cu atoms in orange, N atoms in blue, B atoms in green, H atoms in white, trapped M atom (M@1Vac) in dark red, and trapped M atom (M@2Vac) in red. Since all geometries are identical, for simplicity, we only show those with Cu and Fe in 1Vac and 2Vac, respectively.

Figure 7a shows the reaction energy profile (ΔG_{*nH}) at different H coverages (ranging from *1H to *3H) for systems with different metal dopants (i.e. Cu, Ni, Co, Fe). Considering the first H adsorption step, it is interesting to note that there is a clear energy trend among the different metals: in the case of Cu and Ni, H is strongly bound, whereas in the case of Fe and Co, the H interaction is rather weak and close to thermoneutral.

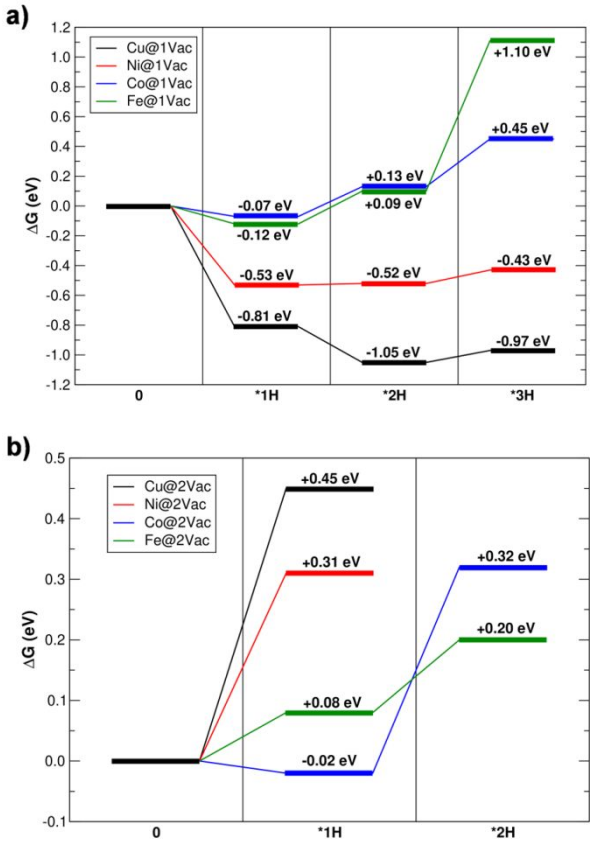

Figure 7. Free-energy diagram (ΔG) for the electrochemical hydrogen adsorption at different H coverage catalyzed by supported metal-doped h-BN systems: (a) filled B monovacancy and (b) filled BN divacancy.

In the case of Cu- and Ni-doped systems, the increase in the coverage leads to a decrease in the differential hydrogen adsorption energy (ΔG_{*H}^{diff}), thus moving closer to the $\Delta G_{*H} \approx 0$ condition at higher coverage, in a similar way as observed for the h-$B^{V}N$/Cu system in the previous section. It is interesting to note the correlation between the M-N bond strength and the reaction energy trend (ΔG_{*nH}) (see discussion in Section 3.1): when the M-N bond is weaker, the H adsorption energy is stronger (i.e. ΔG_{*nH} more negative). This can explain why in the case of Cu- and Ni-dopants, H is strongly bound, whereas in the case of Fe- and Co-dopants, the H interaction is significantly weaker.

In order to assess the feasibility of a *Tafel* mechanism for the hydrogen evolution on isolated metal atoms trapped in a B vacancy, we computed the corresponding activation barrier. This investigation was limited to the case of Ni@1Vac, which is the most promising according to the energy gain of -0.1 eV (*3H to *1H). Unfortunately, as shown in Figure S8, the *Tafel* barrier is computed to be +2.75 eV (electronic energy difference), similarly to what obtained for h-$B^{V}N$/Cu in the previous section. Therefore, again, we are prone to suggest a possible *Heyrovsky* mechanism, where the H_2 molecule evolves through a direct electrochemical step.

We now move to the case of single metal atoms trapped in a BN divacancy (M@2Vac in Figure 6b). In principle, three possible adsorption sites are available for adsorption: the "undercoordinated" N atom, the "undercoordinated" B atom, and the metal atom. We could locate an intermediate where an N-H bond is formed after breaking of one N-M bond (similarly to what observed for the M@1Vac above), but its stability, for all metals considered, is always lower (≈ +0.08/+0.28 eV) than other adsorption sites. We have indeed found a more favorable intermediate, almost identical among all metals, where H binds in a bridging configuration between the metal and the boron atom (see Figure 6b). To shed more light on the interaction between H and Fe@2Vac, in Figure S9, we calculated the charge density difference plot, which proves that the presence of the H atom causes a significant charge redistribution. Here, there is a clear electron charge depletion in the M-B bond and an accumulation between M and H, indicating the formation of an M-H bond. However, some charge accumulation is also located between H and B, indicating that some contribution to the H bond comes from the next B atom.

In Figure 7b we observe that the first electrochemical H adsorption is unfavorable for Cu- and Ni-doped systems, whereas the differential hydrogen adsorption free energy is close to zero for Co- and Fe-doped systems. We may explain these results considering the electronic structure details of the different metal-doped systems, as presented in Section 3.1: differently from the case of Cu and Ni trapped metals, which d states are deeper in energy and thus more stable, Co and Fe d states lie in the proximity of the Fermi energy, which, therefore, are expected to be more reactive for M-H bond formation. We have further analyzed the energy-coverage dependence in the case of the Fe- and Co-doped systems (green and blue lines in Figure 7b), as they are both characterized by the first *differential hydrogen binding energy* close to zero. In the latter case (Fe@2Vac), we found that a possibility to reach a high coverage at a reasonable energy cost exists. For this system,

the activation barrier for the *Tafel* step was found to be +0.96 eV (Figure S10), significantly lower than for the Ni@1Vac case.

4. CONCLUSIONS

In this work, we used dispersion-corrected density functional theory calculations to assess the potential of single metal atoms trapped in defective h-BN on a copper substrate as electrocatalysts for the hydrogen evolution reaction.

Several possible types of interface model systems can be designed when considering various light transition metal atoms, including Cu, Ni, Co, and Fe, as well as various types of h-BN defects (mono- and di-atomic vacancies), as we did in this study. For each model system, we have investigated the structural and electronic properties and we have evaluated the electrochemical stability and activity for HER.

The HER activity was assessed using arguments put forward by the computational hydrogen electrode model, that is the identification of a *differential hydrogen adsorption free energy* close to zero, i.e. $\Delta G_{*H}^{diff} \approx 0$ eV, that is the reference for an ideal electrocatalyst. Interestingly, h-BN/Cu(111) layers with mono- or di-vacancies were found to present differential free adsorption energies close to 0 eV. This is because only the first hydrogen binds very strongly on these systems, whereas the second (or third) hydrogen atoms are weakly adsorbed.

Next, we investigated how the presence of trapped single metal atoms (Cu, Ni, Co, and Fe) may affect the HER activity. Similarly as for defective h-BN/Cu(111), metal-doped h-BN/Cu(111) layers were found to present differential free adsorption energies close to 0 eV. Interestingly, the different metal-doped systems differ for the H coverage required to achieve such a condition. In the case of M@1Vac systems, we have observed a correlation between the N-M strength bond and the ΔG_{*H}^{diff}: when the N-M bond is weaker, the H adsorption is stronger (i.e. a more negative ΔG_{*H}^{diff}).

In both cases, Tafel mechanism barriers were calculated to be high (≈ 1/3 eV), and therefore we may hypothesize a *Heyrovsky* mechanism, in analogy to what previously observed for MoS_2-based catalysts.

Therefore, our results suggest that both defective and single metal-doped h-BN/Cu(111) systems are potentially suitable catalysts for the HER.

Before concluding, we want to compare the systems proposed in this work with MoS_2-based systems, which are considered as the state-of-the-art two-dimensional catalysts for HER.[16] We note some similarities[17] to our results: (1) the MoS_2 basal plane is inert whereas HER activity takes place at extended defects, such as Mo-edges; (2) typically, at low coverage the H atom is too strongly chemisorbed and only the step going from 0.25 to 0.5 ML coverage (corresponding to the differential adsorption free energy, ΔG_{*H}^{diff}) is thermoneutral.

To conclude, the results of the present study could be useful to guide the rational design of h-BN/M interfaces as H_2-evolving electrocatalysts through their defect-engineering and could also stimulate further theoretical as well as experimental investigations in this direction.

ASSOCIATED CONTENT

Supporting Information

The Supporting Information is available free of charge on the ACS Publications website at DOI: evaluation of the electrochemical stability against the metal dissolution in water for the various M@1Vac and M@2Vac systems; Convergence tests for the hydrogen binding energy using a 3-layer and 4-layer models; total (TDOS) and projected (PDOS) density of states of M@1Vac systems; total (TDOS) and projected (PDOS) density of states of M@2Vac systems; energy profile for the flipping of the trapped metal atom in the case of Cu@1Vac and Ni@1Vac, with the corresponding ball-and-stick models of the intermediates and transition states; energy contributions of deformation and of binding to the adsorption energy of metal-doped h-BN/Cu systems; free-energy diagram for the electrochemical H adsorption on pristine and defective h-BN/Cu systems; ball-and-stick models of the intermediates of the H adsorption on pristine and defective h-BN/Cu systems; ball-and-stick models of the intermediates of the H adsorption at different coverages on h-B^VN/Ni; energy profile of Tafel step for free-standing and Cu-supported h-B^VN, with the corresponding ball-and-stick models of intermediates and transition states; energy profile of Tafel step for Ni@1Vac with the corresponding ball-and-stick models of intermediates

and transition state; charge density difference plot for Fe@2Vac; energy profile of Tafel step for Fe@2Vac with the corresponding ball-and-stick models of intermediates and transition state.

ACKNOWLEDGMENTS

This work has been supported by the project "MADAM - Metal Activated 2D cArbon-based platforMs" funded by the MIUR Progetti di Ricerca di Rilevante Interesse Nazionale (PRIN) Bando 2017 - grant 2017NYPHN8. F.S. acknowledges the financial support of the Helmholtz Association.

REFERENCES

[1] Crabtree, G. W., Dresselhaus, M. S., & Buchanan, M. V. (2004). The hydrogen economy. *Physics today*, *57*(12), 39-44.

[2] Barreto, L., Makihira, A., & Riahi, K. (2003). The hydrogen economy in the 21st century: a sustainable development scenario. *International Journal of Hydrogen Energy*, *28*(3), 267-284.

[3] Grigoriev, S. A., Porembsky, V. I., & Fateev, V. N. (2006). Pure hydrogen production by PEM electrolysis for hydrogen energy. *International Journal of Hydrogen Energy*, *31*(2), 171-175.

[4] Turner, J. A. (2004). Sustainable hydrogen production. *Science*, *305*(5686), 972-974.

[5] Seh, Z. W., Kibsgaard, J., Dickens, C. F., Chorkendorff, I. B., Nørskov, J. K., & Jaramillo, T. F. (2017). Combining theory and experiment in electrocatalysis: Insights into materials design. *Science*, *355*(6321), eaad4998.

[6] Greeley, J., Jaramillo, T. F., Bonde, J., Chorkendorff, I. B., & Nørskov, J. K. (2006). Computational high-throughput screening of electrocatalytic materials for hydrogen evolution. *Nature materials*, *5*(11), 909-913.

[7] Nørskov, J. K., Bligaard, T., Logadottir, A., Kitchin, J. R., Chen, J. G., Pandelov, S., & Stimming, U. (2005). Trends in the exchange current for hydrogen evolution. *Journal of The Electrochemical Society*, *152*(3), J23-J26.

[8] Lindgren, P., Kastlunger, G., & Peterson, A. A. (2019). A Challenge to the G~ 0 Interpretation of Hydrogen Evolution. *ACS Catalysis*, *10*, 121-128.

[9] Vesborg, P. C., Seger, B., & Chorkendorff, I. B. (2015). Recent development in hydrogen evolution reaction catalysts and their practical implementation. *The journal of physical chemistry letters*, *6*(6), 951-957.

[10] Wang, H., Tsai, C., Kong, D., Chan, K., Abild-Pedersen, F., Nørskov, J. K., & Cui, Y. (2015). Transition-metal doped edge sites in vertically aligned MoS_2 catalysts for enhanced hydrogen evolution. *Nano Research*, *8*(2), 566-575.

[11] Deng, D., Novoselov, K. S., Fu, Q., Zheng, N., Tian, Z., & Bao, X. (2016). Catalysis with two-dimensional materials and their heterostructures. *Nature nanotechnology*, *11*(3), 218.

[12] Jin, H., Guo, C., Liu, X., Liu, J., Vasileff, A., Jiao, Y., ... & Qiao, S. Z. (2018). Emerging two-dimensional nanomaterials for electrocatalysis. *Chemical reviews*, *118*(13), 6337-6408.

[13] Tang, Q., & Jiang, D. E. (2016). Mechanism of hydrogen evolution reaction on 1T-MoS_2 from first principles. *Acs Catalysis*, *6*(8), 4953-4961.

[14] Zheng, Y., Jiao, Y., Li, L. H., Xing, T., Chen, Y., Jaroniec, M., & Qiao, S. Z. (2014). Toward design of synergistically active carbon-based catalysts for electrocatalytic hydrogen evolution. *ACS nano*, *8*(5), 5290-5296.

[15] Jaramillo, T. F., Jørgensen, K. P., Bonde, J., Nielsen, J. H., Horch, S., & Chorkendorff, I. (2007). Identification of active edge sites for electrochemical H_2 evolution from MoS_2 nanocatalysts. *science*, *317*(5834), 100-102.

[16] Kibsgaard, J., Chen, Z., Reinecke, B. N., & Jaramillo, T. F. (2012). Engineering the surface structure of MoS_2 to preferentially expose active edge sites for electrocatalysis. *Nature materials*, *11*(11), 963.

[17] Hinnemann, B., Moses, P. G., Bonde, J., Jørgensen, K. P., Nielsen, J. H., Horch, S., ... & Nørskov, J. K. (2005). Biomimetic hydrogen evolution: MoS_2 nanoparticles as catalyst for hydrogen evolution. *Journal of the American Chemical Society*, *127*(15), 5308-5309.

[18] Tsai, C., Chan, K., Nørskov, J. K., & Abild-Pedersen, F. (2015). Theoretical insights into the hydrogen evolution activity of layered transition metal dichalcogenides. *Surface Science*, *640*, 133-140.

[19] Huang, Y., Nielsen, R. J., Goddard III, W. A., & Soriaga, M. P. (2015). The reaction mechanism with free energy barriers for electrochemical dihydrogen evolution on MoS_2. *Journal of the American Chemical Society*, *137*(20), 6692-6698.

[20] Zheng, Y., Jiao, Y., Zhu, Y., Li, L. H., Han, Y., Chen, Y., ... & Qiao, S. Z. (2014). Hydrogen evolution by a metal-free electrocatalyst. *Nature communications*, *5*(1), 1-8.

[21] Koitz, R., Nørskov, J. K., & Studt, F. (2015). A systematic study of metal-supported boron nitride materials for the oxygen reduction reaction. *Physical Chemistry Chemical Physics*, 17(19), 12722-12727.

[22] Hu, G., Wu, Z., Dai, S., & Jiang, D. E. (2018). Interface Engineering of Earth-Abundant Transition Metals Using Boron Nitride for Selective Electroreduction of CO_2. *ACS applied materials & interfaces*, 10(7), 6694-6700.

[23] Lyalin, A., Nakayama, A., Uosaki, K., & Taketsugu, T. (2013). Functionalization of monolayer h-BN by a metal support for the oxygen reduction reaction. *The Journal of Physical Chemistry C*, *117*(41), 21359-21370.

[24] Lyalin, A., Nakayama, A., Uosaki, K., & Taketsugu, T. (2013). Theoretical predictions for hexagonal BN based nanomaterials as electrocatalysts for the oxygen reduction reaction. *Physical Chemistry Chemical Physics*, *15*(8), 2809-2820.

[25] Lyalin, A., Nakayama, A., Uosaki, K., & Taketsugu, T. (2014). Adsorption and catalytic activation of the molecular oxygen on the metal supported h-BN. *Topics in catalysis*, *57*(10-13), 1032-1041.

[26] Back, S., & Siahrostami, S. (2019). Noble metal supported hexagonal boron nitride for the oxygen reduction reaction: a DFT study. *Nanoscale Advances*, *1*(1), 132-139.

[27] Zhu, W., Wu, Z., Foo, G. S., Gao, X., Zhou, M., Liu, B., ... & Li, H. (2017). Taming interfacial electronic properties of platinum nanoparticles on vacancy-abundant boron nitride nanosheets for enhanced catalysis. *Nature communications*, *8*(1), 1-7.

[28] Fu, Q., Meng, Y., Fang, Z., Hu, Q., Xu, L., Gao, W., ... & Lu, F. (2017). Boron nitride nanosheet-anchored pd–fe core–shell nanoparticles as highly efficient catalysts for Suzuki–Miyaura coupling reactions. *ACS applied materials & interfaces*, *9*(3), 2469-2476.

[29] Uosaki, K., Elumalai, G., Noguchi, H., Masuda, T., Lyalin, A., Nakayama, A., & Taketsugu, T. (2014). Boron nitride nanosheet on gold as an electrocatalyst for oxygen reduction reaction: theoretical suggestion and experimental proof. *Journal of the American Chemical Society*, *136*(18), 6542-6545.

[30] Uosaki, K., Elumalai, G., Dinh, H. C., Lyalin, A., Taketsugu, T., & Noguchi, H. (2016). Highly efficient electrochemical hydrogen evolution reaction at insulating boron nitride nanosheet on inert gold substrate. *Scientific reports*, *6*, 32217.

[31] Liu, D. Q., Tao, B., Ruan, H. C., Bentley, C. L., & Unwin, P. R. (2019). Metal support effects in electrocatalysis at hexagonal boron nitride. *Chemical communications*, *55*(5), 628-631.

[32] Mao, K., Li, L., Zhang, W., Pei, Y., Zeng, X. C., Wu, X., & Yang, J. (2014). A theoretical study of single-atom catalysis of CO oxidation using Au embedded 2D h-BN monolayer: a CO-promoted O_2 activation. *Scientific reports*, *4*, 5441.

[33] Back, S., Kulkarni, A. R., & Siahrostami, S. (2018). Single Metal Atoms Anchored in Two-Dimensional Materials: Bifunctional Catalysts for Fuel Cell Applications. *ChemCatChem*, *10*(14), 3034-3039.

[34] Cui, Q., Qin, G., Wang, W., Sun, L., Du, A., & Sun, Q. (2019). Mo-doped boron nitride monolayer as a promising single-atom electrocatalyst for CO_2 conversion. *Beilstein journal of nanotechnology*, *10*(1), 540-548.

[35] Tan, X., Tahini, H. A., Arandiyan, H., & Smith, S. C. (2019). Electrocatalytic Reduction of Carbon Dioxide to Methane on Single Transition Metal Atoms Supported on a Defective Boron Nitride Monolayer: First Principle Study. *Advanced Theory and Simulations*, *2*(3), 1800094.

[36] Auwärter, W. (2019). Hexagonal boron nitride monolayers on metal supports: Versatiletemplates for atoms, molecules and nanostructures. *Surface Science Reports*, *74*, 1-95.

[37] Patera, L. L., Bianchini, F., Africh, C., Dri, C., Soldano, G., Mariscal, M. M., ... & Comelli, G. (2018). Real-time imaging of adatom-promoted graphene growth on nickel. *Science*, *359*(6381), 1243-1246.

[38] Carnevali, V., Patera, L. L., Prandini, G., Jugovac, M., Modesti, S., Comelli, G., ... & Africh, C. (2019). Doping of epitaxial graphene by direct incorporation of nickel adatoms. Nanoscale, 11(21), 10358-10364.

[39] Perilli, D., Selli, D., Liu, H., Bianchetti, E., & Di Valentin, C. (2018). h-BN Defective Layers as Giant N-Donor Macrocycles for Cu Adatom Trapping from the Underlying Metal Substrate. *The Journal of Physical Chemistry C*, *122*(41), 23610-23622.

[40] Perilli, D., Selli, D., Liu, H., & Di Valentin, C. (2019). Computational Electrochemistry of Water Oxidation on Metal-Doped and Metal-Supported Defective h-BN. *ChemSusChem*, *12*(9), 1995-2007.

[41] Giannozzi, P., Baroni, S., Bonini, N., Calandra, M., Car, R., Cavazzoni, C., ... & Dal Corso, A. (2009). QUANTUM ESPRESSO: a modular and open-source software project for quantum simulations of materials. *Journal of physics: Condensed matter*, *21*(39), 395502.

[42] Giannozzi, P., Andreussi, O., Brumme, T., Bunau, O., Nardelli, M. B., Calandra, M., ... & Colonna, N. (2017). Advanced capabilities for materials modelling with Quantum ESPRESSO. *Journal of Physics: Condensed Matter*, *29*(46), 465901.

[43] Vanderbilt, D. (1990). Soft self-consistent pseudopotentials in a generalized eigenvalue formalism. *Physical review B*, *41*(11), 7892.

[44] Lee, K., Murray, É. D., Kong, L., Lundqvist, B. I., & Langreth, D. C. (2010). Higher-accuracy van der Waals density functional. *Physical Review B*, *82*(8), 081101.

[45] Hamada, I., & Otani, M. (2010). Comparative van der Waals density-functional study of graphene on metal surfaces. *Physical Review B*, *82*(15), 153412.

[46] Monkhorst, H. J., & Pack, J. D. (1976). Special points for Brillouin-zone integrations. *Physical review B*, *13*(12), 5188.

[47] http://www.webbook.nist.gov (23/07/2020).

[48] Nørskov, J. K., Rossmeisl, J., Logadottir, A., Lindqvist, L. R. K. J., Kitchin, J. R., Bligaard, T., & Jonsson, H. (2004). Origin of the overpotential for oxygen reduction at a fuel-cell cathode. *The Journal of Physical Chemistry B*, *108*(46), 17886-17892.

[49] Henkelman, G., Uberuaga, B. P., & Jónsson, H. (2000). A climbing image nudged elastic band method for finding saddle points and minimum energy paths. *The Journal of chemical physics*, *113*(22), 9901-9904.

[50] Löwdin, P. O. (1955). Quantum theory of many-particle systems. I. Physical interpretations by means of density matrices, natural spin-orbitals, and convergence problems in the method of configurational interaction. *Physical Review*, *97*(6), 1474.

[51] Kokalj, A. (1999). XCrySDen—a new program for displaying crystalline structures and electron densities. *Journal of Molecular Graphics and Modelling*, *17*(3-4), 176-179.

[52] Wang, Y., Mao, J., Meng, X., Yu, L., Deng, D., & Bao, X. (2018). Catalysis with two-dimensional materials confining single atoms: concept, design, and applications. *Chemical reviews*, 119(3), 1806-1854.

[53] Hansen, H. A., Rossmeisl, J., & Nørskov, J. K. (2008). Surface Pourbaix diagrams and oxygen reduction activity of Pt, Ag and Ni (111) surfaces studied by DFT. *Physical Chemistry Chemical Physics*, *10*(25), 3722-3730.

For Table of Contents Only